GEOPHYSICS, VOL. 55, NO. 2 (FEBRUARY 1990); P. 147–156, 13 FIGS.

Reflection shear-wave data collected near the principal axes of azimuthal anisotropy

H. B. Lynn* and L. A. Thomsen‡

ABSTRACT

The presence of vertically oriented fractures and/or unequal horizontal stresses has created an azimuthally anisotropic earth, in which shear-wave (*SH*) data collected along the principal axes of the anisotropy display time and reflection amplitude anomalies.

Amoco shot two crossing shear-wave (*SH*) lines that were approximately parallel to the orthogonal principal axes of the azimuthal anisotropy. At the tie point, these crossing *SH* lines display a time-variant mis-tie. The tie point also displays reflection-coefficient anomalies, attributable to azimuthally dependent shear-wave velocities. Field mapping documented a set of fractures striking N69E which are approximately parallel to the line that exhibited greater traveltimes. Time-variant mis-ties and reflection coefficient anomalies are two of the seismic responses theoretically expected of an azimuthally anisotropic earth, i.e., one in which the shear-wave velocity depends upon the polarization azimuth of the shear wave.

INTRODUCTION

The effect of oriented cracks or unequal horizontal stresses on shear-wave velocities and particle motion has been discussed in the literature for many years. Nur and Simmons (1969) reported uniaxial stress laboratory experiments on granite samples. The closing of cracks in some directions and opening of cracks in other directions was seen as the cause of acoustic double refraction, in which two shear waves travel at different velocities. Nur (1971) further computed the theoretical effects of stress on velocity anisotropy in the presence of cracks. Lo et al. (1986) have published laboratory measurements of anisotropy in sedimentary and granitic rocks. Rai and Hanson (1988) published the azimuthal anisotropy observed in a few samples of sandstones, limestones, and shales. They reported, as did the earlier lab studies, that the magnitude and nature of the applied stress (hydrostatic and/or uniaxial) govern the magnitude of the observed birefringence. Sondergeld and Rai (1987) reported lab observations of shear-wave splitting and demonstrated the equivalence between physical rotation of sources and receivers and mathematical rotation of a properly acquired data set as proposed by Alford (1986a, b).

Crampin (1981, 1984, 1985a and references therein) has written on anisotropy for at least 15 years, developing the theoretical aspects. Crampin (1985b) and Crampin et al. (1985) documented field evidence of shear-wave splitting in earthquake seismic records, verifying earlier insights by Gupta (1973). Crampin's recent articles (1986, 1987, 1988) stress the importance of the splitting phenomena to exploration geophysics, i.e., that the polarization of the first arrival is parallel to the fracture strike direction. He has proposed "extensive-dilatancy-anisotropy (EDA)," resulting from stress-aligned, fluid-filled microcracks, as the major cause of the splitting. Thomsen (1986a and 1988) presented a set of equations which govern wave propagation in weakly anisotropic rocks and has specialized them (Thomsen, 1986b) to describe aligned cracks or joints in porous rock.

At the 1986 International SEG convention, there were 11 papers on shear-wave azimuthal anisotropy, presented by Amoco, Exxon, Chevron, CGG, and the British Geological Survey (see especially Willis et al., 1986). During the 1987 International SEG convention, 17 papers were presented. Our capability to use seismic data to determine the direction of oriented fractures is a major technological breakthrough and deserves to be widely discussed, noted, and used in appropriate situations and plays. Modeling of shear-wave splitting is useful for interpretation and processing purposes. Preacquisition modeling would also be appropriate in order to adjust the acquisition parameters and locations.

In this paper, we discuss shear-wave (*SH*) reflection field data in which oriented fractures and/or unequal horizontal

Presented at the 56th Annual International Meeting, Society of Exploration Geophysicists. Manuscript received by the Editor June 14, 1988; revised manuscript received August 8, 1989.
*Lynn Incorporated, 1642 Fall Valley Drive, Houston, TX 77077.
‡Amoco Production Company, P.O. Box 3385, Tulsa, OK 74102.

stresses caused an azimuthally anisotropic response of the earth to be recorded. Two crossing colocated *P*- and *SH*-wave lines were acquired in Pennsylvania (Figure 1). A few concepts concerning the shear-wave responses to azimuthal anisotropic media are presented briefly before the data are examined (see also Lynn, 1986).

Azimuthal anisotropy exists in the presence of oriented fractures or unequal horizontal stresses (see Figure 2). Two principal axes are defined: parallel to ($S1$) and perpendicular to ($S2$) the vertically oriented fractures or microfractures. The horizontal stresses associated with this fracture trend are the maximum horizontal stress (parallel to the fracture trend) and the minimum horizontal stress (perpendicular to the fractures). For vertical propagation, the $S1$ shear wave polarized parallel to the vertical oriented fractures travels at the faster velocity; the $S2$ shear wave polarized perpendicular to the fractures travels at the slower velocity. These vertical shear-wave velocities thus depend upon polarization direction with respect to the natural axes of the anisotropy.

In most surveys, the acquisition lines lie at arbitrary angles to the principal axes, as was discussed by Alford (1986a, b). In this general case, the shear signal emitted from the source, upon encountering the anisotropic region, splits into two waves. The faster traveling wave ($S1$) has particle motion parallel to the fractures, and the slower traveling wave ($S2$) has particle motion perpendicular to the fractures (Crampin, 1985a). This paper discusses the simpler results observed when two crossing *SH* lines happened to lie close to the principal axes of the anisotropy, so that the shear-wave energy did not split significantly.

SH particle motion is transverse to the line direction, as shown in Figure 2; *SV* particle motion is inline. These terms are used to describe the source polarization; they may also be used to describe the wave polarization only when the medium is azimuthally isotropic, or (as here) when the survey lines lie near the principal directions of azimuthal anisotropy. The conventional field-acquisition terms of "*SH*" and "*SV*" are at best insufficient for discussing the data acquired in azimuthally anisotropic media. Instead, map-consistent particle-motion directions should be used during the processing and analysis steps.

Figure 3a schematically illustrates the effect of azimuthal anisotropy on shear-wave data. A formation at a given depth z reflects the two differently polarized shear waves. Almost vertically incident raypaths are shown. When, for example, the east-west velocity is different from the north-south velocity, then different shear-wave traveltimes to the same reflector are recorded, as shown in Figure 3b. When the entire sedimentary column is azimuthally anisotropic, to varying degrees, and the principal axes do not change direction with depth, then the zero-offset traveltime differences between correlative reflectors tend to increase with depth (or time), causing a dynamic traveltime difference. Thomsen (1986a, 1988) has discussed the shear traveltimes for significant offsets [the normal-moveout (NMO) velocities] through azimuthally anisotropic media. This paper discusses the CDP stacked trace, which is an approximation to zero-offset (vertical) data.

The two anomalies we observed on the data were (a) a dynamic or time-variant mis-tie and (b) azimuthally dependent reflection amplitudes. When velocity is a function of azimuth, it is easy to see that the reflection coefficients may also change with azimuth, as may the recorded amplitudes.

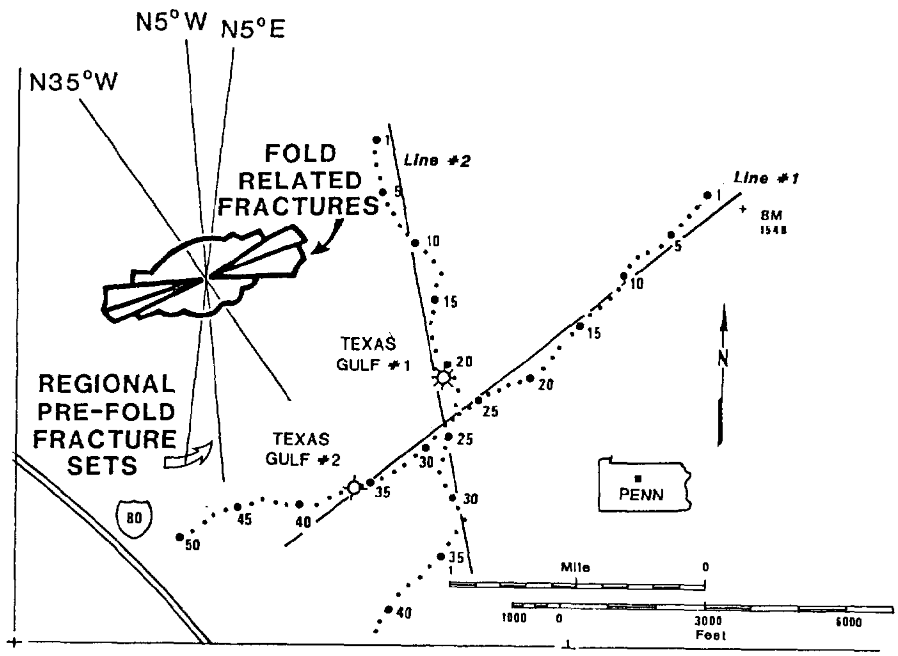

FIG. 1. Base map for *P* and *SH* seismic lines and wells, with rose diagram of strikes of fold-related fractures mapped in outcrop.

Field data acquisition

In September of 1980, Amoco acquired two colocated *P*- and *SH*-wave lines in Pennsylvania, with 48-channel field recording (see Figure 1). Tests for the *P* and *SH* waves were performed along line 1 (east-west) to determine field parameters. The group spacing was 280 ft; the group array length was 360 ft; every group was shot. Line 1 was 2.5 miles long; line 2 was shorter (about 2 miles) due to terrain difficulties. For the *P* data, four inline vibrators were used, with 100 ft spacing. At each vibrator point (VP), sixteen 14–56 Hz sweeps were taken with a 14 s upsweep. The receiver array comprised 36 vertical phones, 10 ft apart. For the shear data, four *SH* vibrators with 100 ft spacing were used. The shear sweep was a 4–32 Hz upsweep over 14 s, and 32 sweeps per VP were taken. The *SH* receiver arrays used horizontal geophones in the *SH* orientation with the same dimensions, layouts, and ground locations as the vertical geophones.

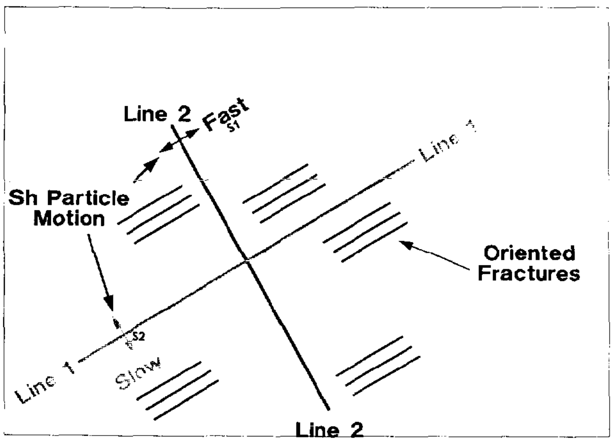

FIG. 2. *SH* lines lying close to the principal axes: the *SH* wave with particle motion parallel to the fractures travels at the faster velocity; the *SH* wave with particle motion perpendicular to the fractures travels at the slower velocity.

Data processing summary

The *P*-wave data needed no special processing; standard processing yielded excellent results. The shear data required iterative processing, which is described next.

In the initial *SH* processing, the reference-to-datum velocity was 7000 ft/s, which was an average of the *SH* first-break velocity and one-half the *P* reference-to-datum velocity. The initial *SH* stacking velocity was one-half the *P* stacking velocity applied at twice the *P*-wave time, which is the customary rough estimate of a 2:1 conversion factor from *SH* to *P*. Residual NMO was then removed to flatten the hyperbolas approximately. CMP sort, moveout, statics, and stack provided brute sections. The resulting brute stacks showed an approximate V_p/V_s ratio of 1.8:1 from *SH* to *P*, so the data were moved out again using the 1.8 ratio and residual NMO picked.

The automatic statics program (as well as the hand-picked statics for the largest static values) were iterated and provided an estimate of the high-frequency static corrections.

With the initial estimates of statics and stacking velocities accomplished, we studied the reference-to-datum velocity. By applying to the data a suite of closely spaced reference-to-datum velocities and choosing the one deemed to give the best results, we found an optimum *SH* reference to datum velocity of 4300 ft/s. The stacking velocities and the statics were then reestimated *directly from the S-wave data*, after applying the new reference velocity.

In the final estimation of *SH* and *P* residual statics, we found that a relationship existed on line 1 between the *P* and *SH* residual statics. We cross-plotted the statics and determined that the ratio of *SH*-to-*P* static values (after reference to datum statics) was 2.79. Interestingly enough, 2.79 was also the ratio of the *P* reference velocity to *SH* reference velocity (12 000/4300), suggesting on line 1 that whatever was causing the residual *P* static was also causing the residual *SH* static and that the V_p/V_s ratio of that zone was 2.79. A V_p/V_s ratio of this size is not unusual in the upper 3000 ft of sedimentary rock (Nicholson and Simpson, 1985). On line 2, there was no clear-cut correlation between *P* and

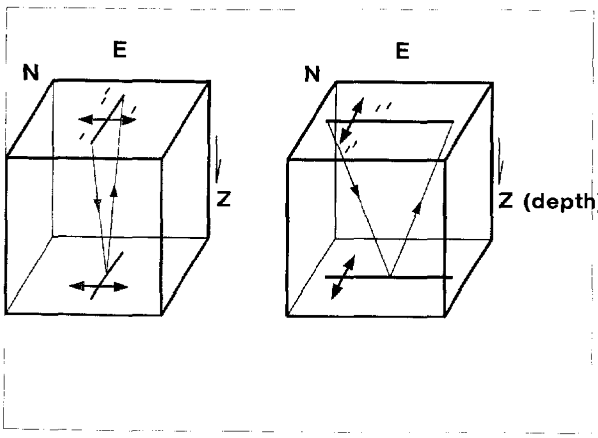

FIG. 3(a). Schematic diagram, showing shear travel paths in depth z for one reflector at a given depth. The trend of the vertically oriented cracks is shown to be east-west.

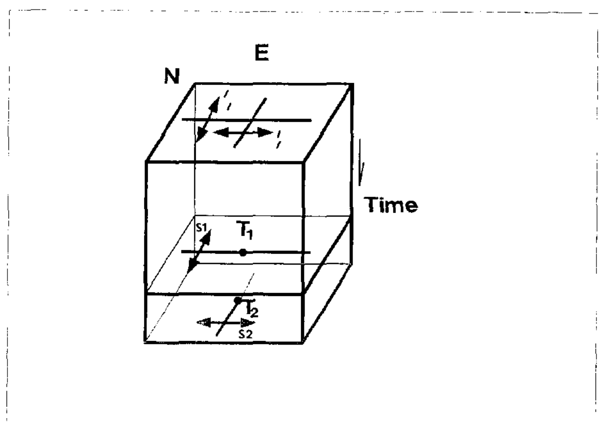

FIG. 3(b). Schematic diagram showing correlative shear traveltimes t_1 and t_2 to the reflector in (a), in an azimuthally anisotropic earth.

SH residual statics. The final CDP gathers showed that the NMO and the statics we applied had correctly transformed the offset times into the zero-offset time.

Velocity filtering (*f-k* filtering) of the common-shot records after achieving the best possible processing, up to but not including stack, yielded significantly improved data.

Two final stacks per *SH* line were made, creating both a relative true-amplitude stack, as much as possible for land data, and a spectral-whitened stack. The final stacks were migrated using an *f-k* migration algorithm. The two lines required different stacking velocities and different migration velocities in order to achieve correct imaging.

The final sections are displayed in Figures 4 and 5. Line 1 (Figure 4) is approximately a strike line and has quite good data quality. The *SH* time scale is compressed using a V_p/V_s ratio of 1.8, which appears to be the best average V_p/V_s ratio for the entire sedimentary column (about 20 000 ft of section). Line 2 (Figure 5), the dip line, was of poorer data quality, yet the target at about 12 000 ft is sufficiently well imaged. On the migrated data, the anticline in the subsurface at about 1.3 s *P*-wave time is visible.

Interpretation

The *P*-wave reflectors were identified using synthetic seismograms from the well on line 1 and the check-shot survey in the well. The *SH* reflectors were character-correlated by eye to the *P* reflectors. There was a very strong similarity in the reflectors down to about 18 000 ft depth (about 2.3 s *P*-wave time); below that depth, the dramatic visual similarity was missing; and the *P-SH* correlation was much less well assured.

The two *P*-wave lines tied without a problem (Figure 6). The tie point of the *SH* lines (Figure 7) exhibits a time-variant mis-tie, evident on both the stack and the migrated section. Event A, a limestone marker at about 1.5 s shear time (6200 ft depth), shows a 21 ms mis-tie between the two sections on Figure 7. Event B, the top of a presumed Cambrian clastic section near 4.35 s, displays a mis-tie of 61 ms. The estimated depth of this reflector is 20 000 ft. For both of these events, the mis-ties imply a 1.4% average anisotropy. A series of figures in which different static shifts were applied in order to align these events are now presented.

Event A is aligned in Figure 8, and now the 21 ms mis-tie is evident at time zero, as well as the residual 40 ms mis-tie at the Cambrian level. Aligning the Cambrian-basement section (event B) in Figure 9 demonstrates the excellent character tie at event B and the 40 ms mis-tie at event A. On these two lines, the reflections from the same horizon at depth arrive at the tie point with different traveltimes.

Since line 1 and line 2 are not *perfectly* aligned in the principal directions of anisotropy, there is undoubtedly some shear-wave splitting with both fast and slow shear waves being recorded on each line. For example, on Figure 7 and Figure 9, it is possible to interpret a tie between the deep fast-to-fast and slow-to-slow reflections (between 3 to 5 s) at the tie point.

The major argument for the time-variant mis-tie is summarized in Figure 10, concentrating on data between 1.5 to 2.5 s. We have shifted line 1 up about 48 ms in order to align the target formation. The events on line 1 display greater interval transit times between correlative reflectors than the interval transit times on line 2. This time-variant mis-tie results from a different velocity function for north-south polarization than for east-west polarization. The amplitude differences along the circled reflector are discussed below.

Naturally, we examined the CDP gathers to verify that the zero-offset times were different in a time-variant mode at the tie point. Figure 11 shows the gathers from the tie point with event A aligned. The gathers show that the hyperbolic events are flattened to the zero-offset time and that the zero-offset times are misaligned at event B by 41 ms. For the reflections between events A and B, the mis-tie smoothly increases to the 41 ms mis-tie at depth. All the gathers on these two lines were carefully scrutinized for any indications of error in processing or in acquisition.

The dynamic mis-tie was not caused by human or machine error. Something in the earth caused a different vertical shear velocity for polarization north-south than for polarization east-west. This condition is termed azimuthal anisotropy. Briefly, when the shear velocity is anisotropic, it is due to the shear modulus, since bulk density is an isotropic quantity:

$$V_{\text{shear}} = \sqrt{\frac{\mu_{\text{effective}}}{\rho}}.$$

The effective shear modulus in the presence of oriented fractures is a function of azimuth. The effective modulus is defined by

$$\mu_{\text{effective}} = \frac{\text{shear stress (force/area)}}{\text{shear strain (deformation)}}.$$

For a given shear stress, different deformations or strains result, depending upon whether the shear stress applied is parallel or perpendicular to the fractures (Figure 12). The difference in shear velocity depends upon the fracture density ε:

$$\varepsilon = \frac{3\ \text{(fracture porosity)}}{4\pi\ \text{(aspect ratio)}},$$

where aspect ratio is the crack width divided by the crack length.

Were there oriented fractures in the acquisition area? Yes, there were. Amoco geologists did extensive field mapping of fold and fold-related fracture patterns in and around the acquisition area. The strikes of the fractures they mapped are displayed in a rose diagram form upon the base map in Figure 1. These fold-related fracture sets are associated with the Appalachian orogeny. The preponderance of fold-related fractures strike about N69E and are approximately parallel to line 1. This line, in which the *SH* particle motion was perpendicular to those fractures, showed the greater interval transit times to correlative reflectors, i.e., the slower velocities.

However, the geologists had determined from cores and borehole televiewers that the pay in the target sandstones was in the prefold regional fracture system oriented north-south, as shown in Figure 1. After these cracks opened up,

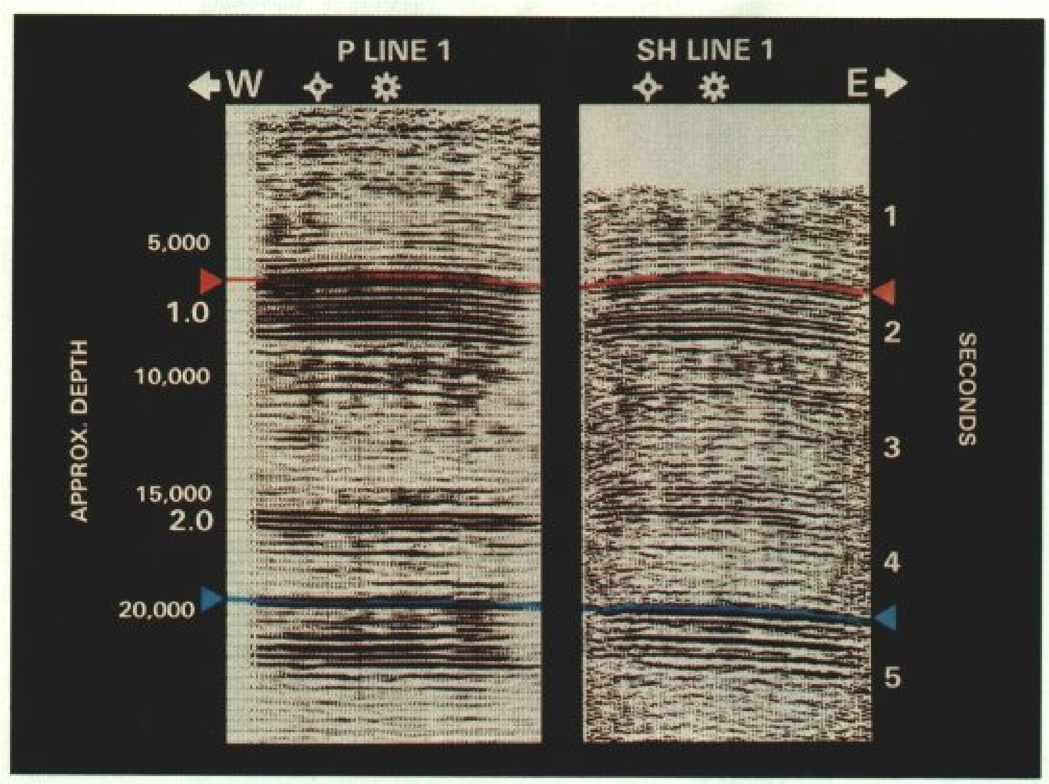

FIG. 4. Line 1, *P* and *SH*, is the strike line. It crosses line 2 in the center.

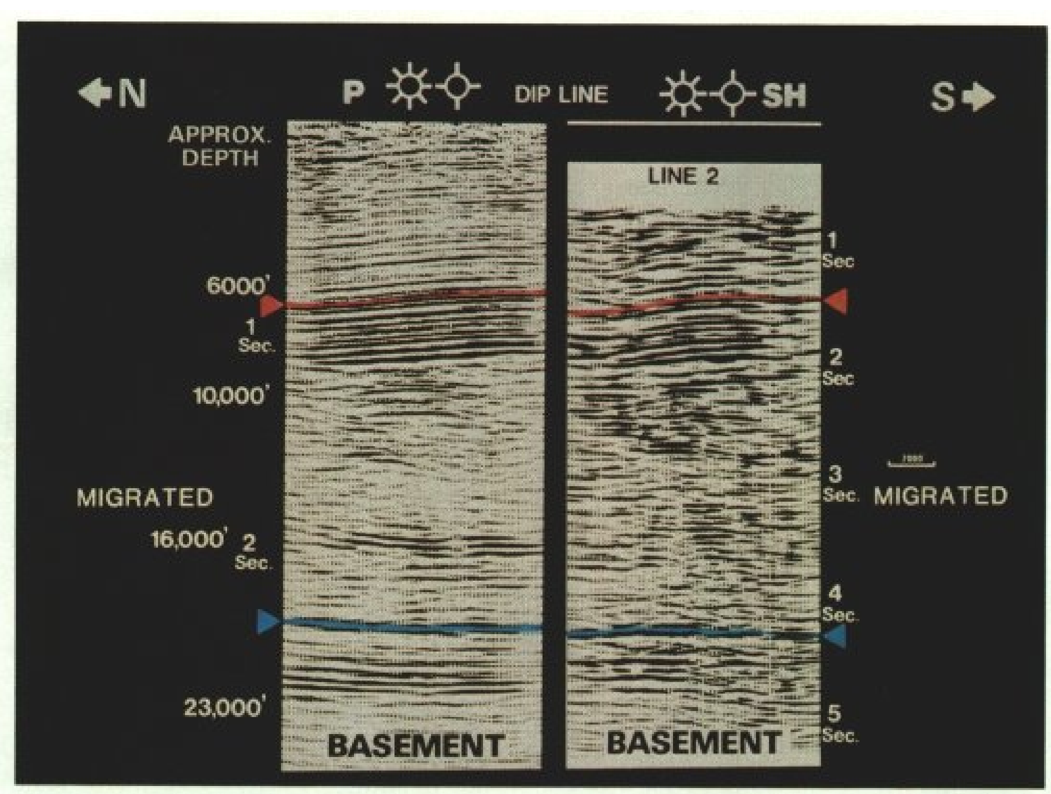

FIG. 5. Line 2, *P* and *SH*, is the dip line. It crosses line 1 in the center.

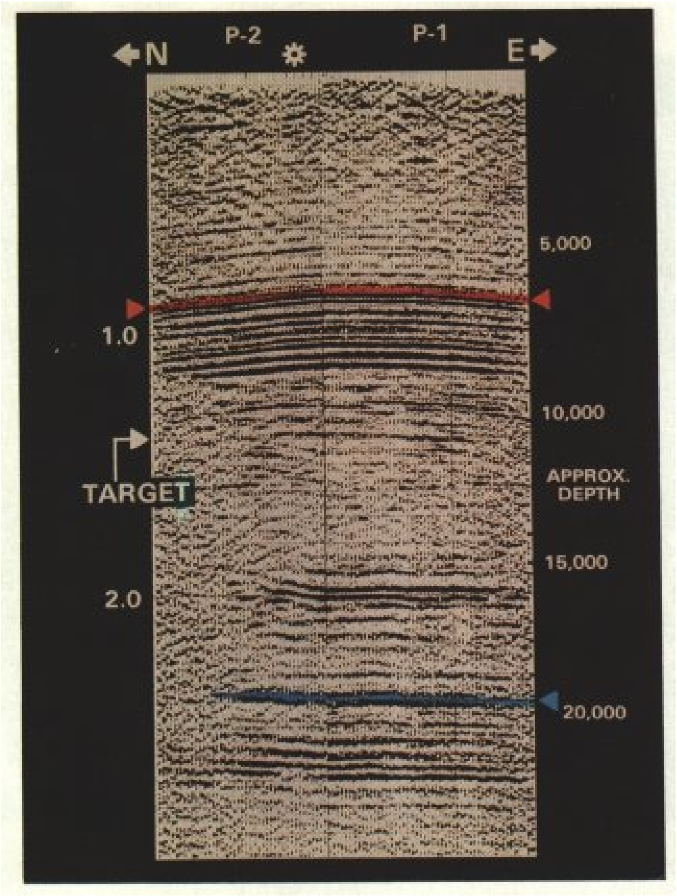

FIG. 6. The two *P*-wave lines spliced at their tie point.

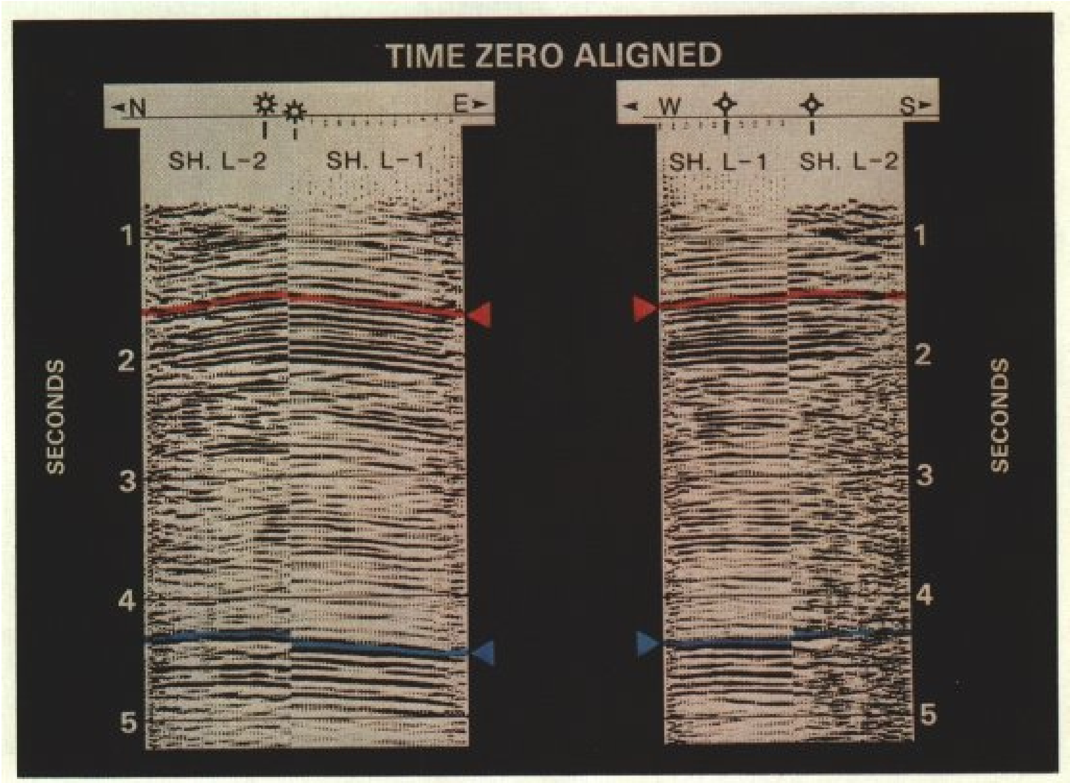

FIG. 7. The two *SH*-wave lines spliced at their tie point do not tie. (Time-zero aligned, timing lines aligned.)

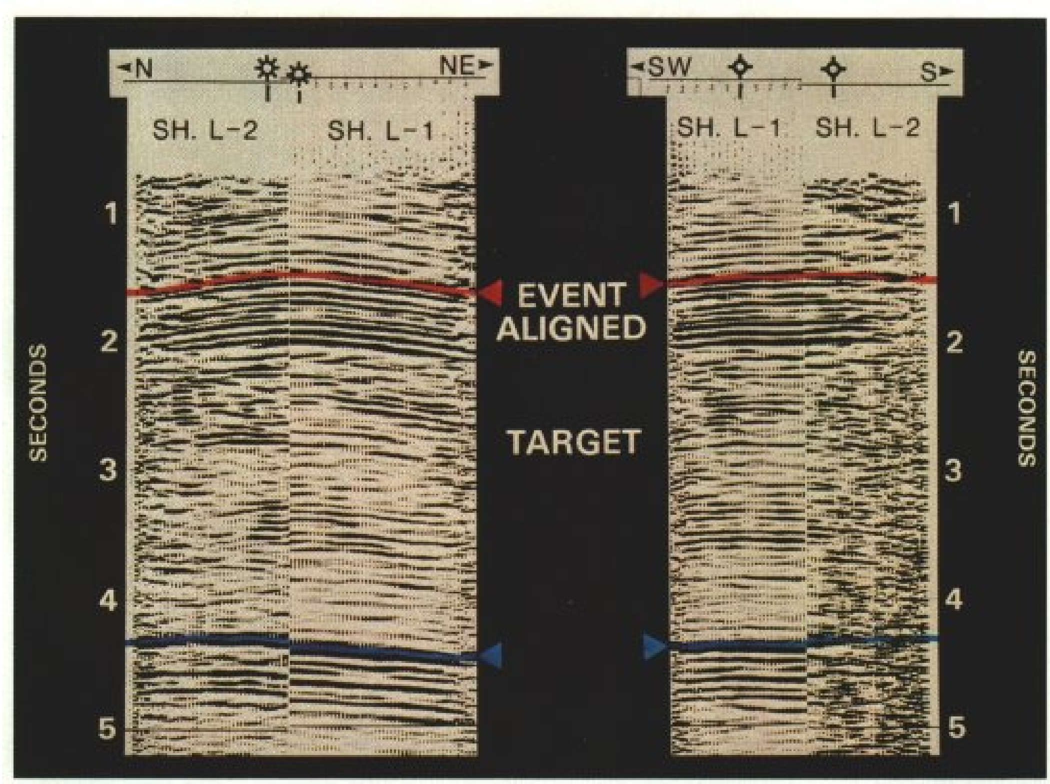

FIG. 8. *SH* tie point with event A in red aligned.

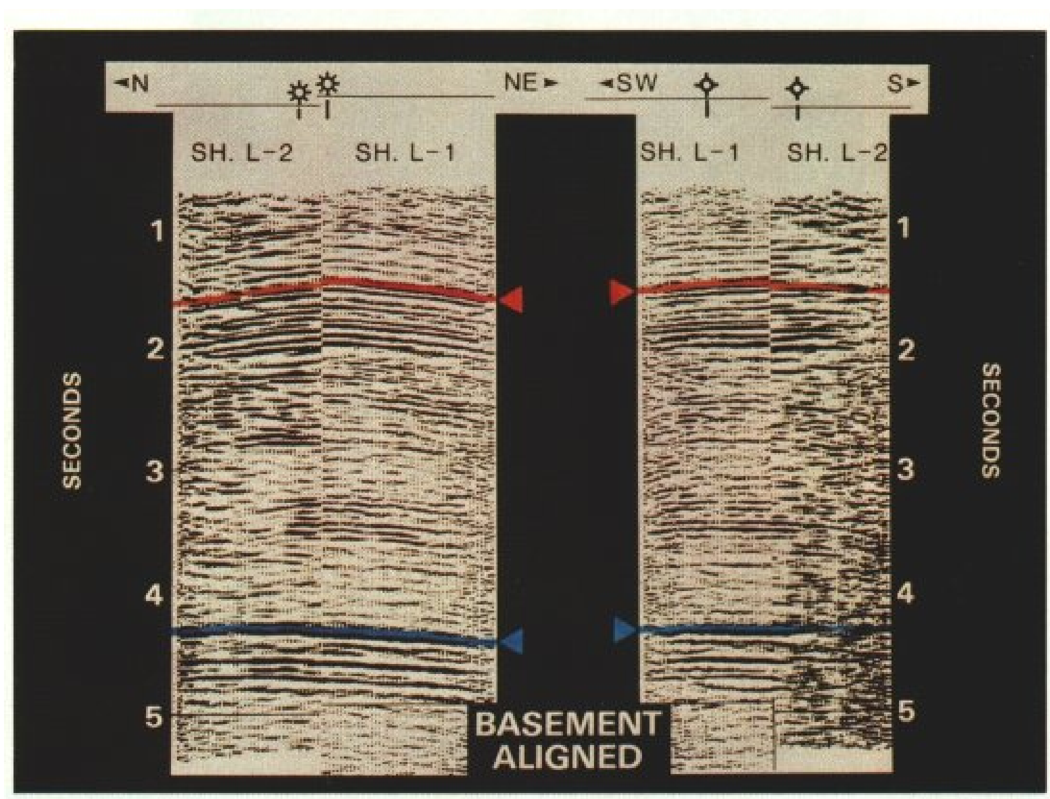

FIG. 9. *SH* tie point with event B in blue (presumed Cambrian through basement reflections) aligned.

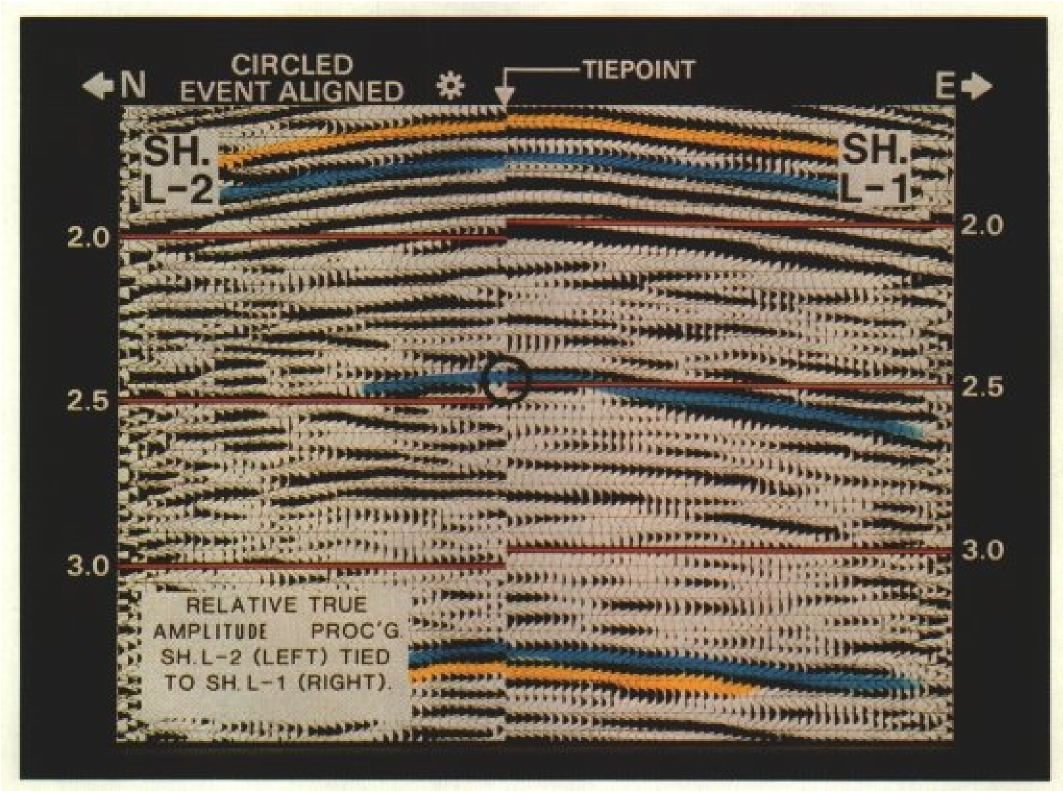

FIG. 10. *SH* data shown between about 1.7 to 3.5 s. The events exhibit a time-variant mis-tie and reflection coefficient differences. The target zone is circled.

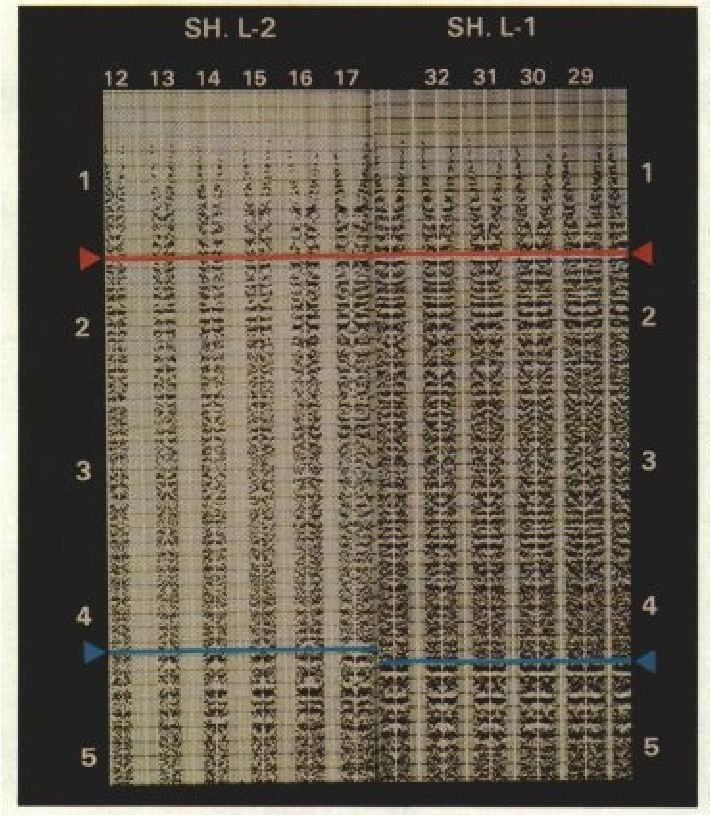

FIG. 11. *SH* CDP gathers with NMO and statics applied. Event A in red has been aligned. Note the 21 ms mis-tie of timing lines (time zero). The events have been corrected to the zero-offset times and the zero-offset times exhibit a time variant mis-tie.

quartz crystals were precipitated in them, holding them open during the subsequent orogeny and changing stress fields. How can one detect these zones of partially mineralized open north-south oriented fractures at target level?

The reflection amplitudes on line 2 contain the pertinent information: where the effective shear velocity of the sandstone is lowered by fractures, it approaches that of the overlying shale and the reflection coefficients are decreased. We analyzed line 2 for reflection coefficient changes related to north-south fractures, because on that line, the particle motion is perpendicular to the relevant fractures. At the tie point, where we have our best measurement of the response to orthogonally polarized shear waves, we see that the lines displayed different reflection amplitudes at the target (Figure 10). This difference was on the order of 9 dB. We relate that difference in reflection coefficient to different effective shear velocities at the target level. We modeled a 9 dB difference to determine the difference in shear velocities and what the fracture density would be.

The model for the calculations, shown in Figure 13, used a low-velocity shale overlying a fractured gas-filled sandstone. The shale most likely possesses vertical transverse isotropy, but for vertical incidence, that is not relevant. The uncracked sandstone S-wave velocity is 11 000 ft/s; the cracked sandstone S-wave velocity is 9100 ft/s, a 17% change. The P-wave velocities and the densities came from the well data, and the shear velocity for the shale came from the shear seismic data. In the graph, the reflection coefficient for P and shear waves as a function of the angle between the survey line and the fractures is presented. At 0 degrees between the SH line and the fractures, the SH particle motion is across the fractures. Thus, a slow shear velocity in the sandstone results; the velocity change between the shale and the fractured sandstone is small; and a small reflection coefficient is recorded. When the line is at 90° to the fractures, the SH polarization senses the uncracked sandstone velocity, so the velocity change between the shale and the uncracked sandstone is larger, and the reflection coefficient increases to about 0.13, which is a 9 dB increase.

For land data, it is well known that producing a true relative-amplitude stack is difficult. At the tie point, the amplitude differences at the target zone could be influenced by raypath effects, different source-receiver properties, coupling, etc. Inasmuch as we could, we accounted for such factors in processing. We believe that azimuth-dependent reflection coefficients are a natural consequence of azimuthally anisotropic media, although the demonstration using crossing SH lines, as was done here, inevitably raises questions of possible confusion between anisotropy and lateral heterogeneity.

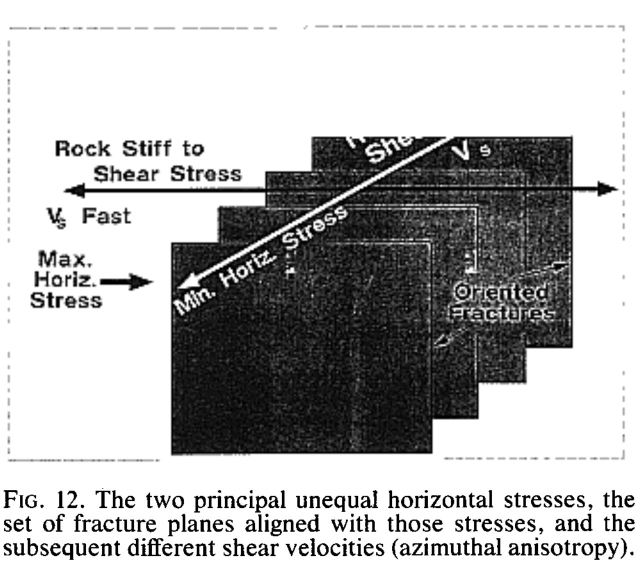

FIG. 12. The two principal unequal horizontal stresses, the set of fracture planes aligned with those stresses, and the subsequent different shear velocities (azimuthal anisotropy).

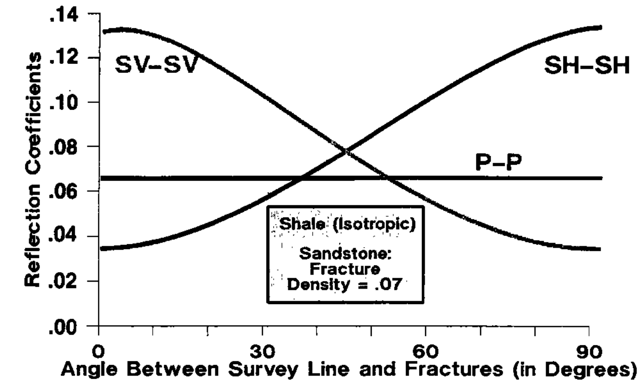

FIG. 13. The model for calculating the change in reflection coefficient, and the graph of reflection coefficients (normal incidence) plotted against angle between survey line and fractures.

It is far more practical to compare colocated shear-wave data gathered or processed to lie along the principal natural axes of the anisotropy, rather than to compare tie points of SH lines. A single colocated SH and SV line, correctly acquired and processed by rotation to lie in the natural coordinate system (Alford, 1986a, b), can demonstrate time and amplitude anomalies along the line, anomalies from which the azimuth of the fractures could be determined, and the fracture density estimated via modeling. This technique is preferred; however, the current data set is of interest nevertheless because it was the first in which the phenomena were apparent in the context of petroleum exploration and because the phenomena are simpler when the data are collected near the principal axes of anisotropy.

The *P*-wave data

For vertical incidence, the P-wave energy is unaffected by azimuthal anisotropy. However, on the far offsets, if the P-wave particle motion crosses the fracture planes, the P wave will travel at a slower velocity. The P-wave far-offset events that have particle motion parallel to the fractures travel at the faster (uncracked) velocity. Although we observed a significant difference in P-wave stacking velocities at the tie point consistent with our understanding of P-wave propagation through this cracked medium, the possible presence of heterogeneity and the different elevation changes on line 1 and line 2 preclude our attributing these observations to anisotropy. Line 1 had about 500 ft of elevation changes from the start of the line to the middle of the line, while line 2 had about 300 ft of elevation change from the start to the middle of the line. As Thomsen (1986a,

1988) has pointed out, P-wave anisotropy in azimuthally anisotropic media must be determined from traveltimes over different raypaths. Heterogeneity may occur on the different raypaths, which can mask or make invalid the attempts to discern the effects of anisotropy on P-wave data.

SUMMARY

We believe that this field data set is important in that it is the first published data which demonstrate shear-velocity anisotropy in an exploration context. The vertical velocities at the tie point of the two SH wave lines depend upon the polarization direction of the shear wavefront. The azimuthal anisotropy present is attributed to oriented fractures and/or unequal horizontal stresses associated with folding during the Appalachian orogeny.

From numerous laboratory experiments and theoretical work, we know that oriented fractures or unequal horizontal stresses can cause shear-wave velocity anisotropy. The faster shear-wave polarization is parallel to the fractures; the slower shear-wave polarization is perpendicular to the fractures. The use of shear-wave anisotropy to measure the orientation and density of vertical aligned fractures in the subsurface is seen to be a viable and worthwhile technique.

ACKNOWLEDGMENTS

This work was performed in 1980–1982 when both authors were employed by Amoco Production Company. The authors thank Amoco for releasing this work for publication.

REFERENCES

Alford, R. M., 1986a, The effects of azimuthal anisotropy on shear-wave data: Presented at the 48th Mtg., Eur. Assn. Expl. Geophys.

——— 1986b, Shear data in the presence of azimuthal anisotropy Dilley, TX: 56th Ann. Internat. Mtg., Soc. Expl. Geoph., Expanded Abstracts 476–479.

Crampin, S., 1981, A review of wave motion in anisotropic and cracked elastic-media: Wave Motion, **3**, 343–391.

——— 1984, An introduction to wave propagation in anisotropic media, *in* Crampin, S., Hipkin, R. G., and Chesnokov, E. M., Eds., Proc. of the 1st Internat. Workshop on Seismic Anisotropy, Suzdal, 1982: Geophys. J. Roy. Astr. Soc., **76**, 17–28.

——— 1985a, Evaluation of anisotropy by shear-wave splitting: Geophysics, **50**, 142–152.

——— 1985b, Evidence for aligned cracks in the Earth's crust: First Break, **3**, 12–15.

——— 1986, Anisotropy and transverse isotropy: Geophys. Prosp., **34**, 94–99.

——— 1987, The geological and industrial implications of extensive-dilatancy anisotropy: Nature, **328**, 491–496.

——— 1988, Nonparallel S-wave polarizations in sedimentary basins: 58th Ann. Internat. Mtg., Soc. Expl. Geophys., Expanded Abstracts 1130–1132.

Crampin, S., Evans, R., and Ucer, S. B., 1985, Analysis of records of local earthquakes: the Turkish dilatancy projects (TDP1 and TDP2): Geophys. J. R. Astr. Soc., **83**, 1–16.

Gupta, I. N., 1973, Preliminary variations in S-wave velocity anisotropy before earthquakes in Nevada: Science, **182**(4117), 1129.

Lo, T-W., Coyner, K. B., and Toksöz, M. N., 1986, Experimental determination of elastic anisotropy of Berea sandstone, Chicopee shale, and Chelmsford granite: Geophysics, **51**, 164–171.

Lynn, H. B., 1986, Seismic detection of oriented fractures: Oil and Gas J., **84**, (Aug. 4), 54–55.

Nicholson, C., and Simpson, D. W., 1985, Changes in V_p/V_s with depth: Bull. Seis. Soc. Am., **75**, 1105–1123.

Nur, A., and Simmons, G., 1969, Stress-induced velocity anisotropy in rocks—An experimental study: J. Geophys. Res., **74**, 6667–6674.

Nur, A., 1971, Effects of stress on velocity anisotropy in rocks with cracks: J. Geophys. Res., **76**, 2022–2034.

Rai, C. S., and Hanson, K. E., 1988, Shear-wave velocity anisotropy in sedimentary rocks: A laboratory study: Geophysics, **53**, 800–806.

Sondergeld, C. H., and Rai, C. S., 1987, Determination of elastic symmetry in rock utilizing shear birefringence: EOS, Trans. Am. Geophys. Union, **68**, 1502.

Thomsen, L., 1986a, Weak elastic anisotropy: Geophysics, **51**, 1954–1966.

——— 1986b, Elastic anisotropy due to aligned cracks: Theoretical models: Trans. Am. Geophys. Union, **67**, 1207.

——— 1988, Reflection seismology over azimuthally anisotropic media: Geophysics, **53**, 304–313.

Willis, H. A., Rethford, G. L., and Bielanski, E., 1986, Azimuthal anisotropy: Occurrence and effect on shear wave data quality: 56th Ann. Internat. Mtg., Soc. Explor. Geophys., Expanded Abstracts, 479–480.